IEEE Access
Multidisciplinary | Rapid Review | Open Access Journal

Received May 20, 2022, accepted June 12, 2022, date of publication June 16, 2022, date of current version June 23, 2022.

Digital Object Identifier 10.1109/ACCESS.2022.3183635

Voltage/Frequency Regulation With Optimal Load Dispatch in Microgrids Using SMC Based Distributed Cooperative Control

SHAFAAT ULLAH[1,2], LAIQ KHAN[3], IRFAN SAMI[4], AND JONG-SUK RO[4,5]

[1]Department of Electrical and Computer Engineering, COMSATS University Islamabad, Abbottabad Campus, Abbottabad, Khyber Pakhtunkhwa 22060, Pakistan
[2]Department of Electrical Engineering, University of Engineering and Technology Peshawar, Bannu Campus, Bannu, Khyber Pakhtunkhwa 28100, Pakistan
[3]Department Electrical and Computer Engineering, COMSATS University Islamabad, Islamabad 45550, Pakistan
[4]School of Electrical and Electronics Engineering, Chung-Ang University, Dongjak-gu, Seoul 06974, Republic of Korea
[5]Department of Intelligent Energy and Industry, Chung-Ang University, Dongjak-gu, Seoul 06974, Republic of Korea

Corresponding author: Jong-Suk Ro (jongsukro@gmail.com)

This work was supported in part by the National Research Foundation of Korea (NRF) funded by the Korean Government [Ministry of Science and ICT (MSIT)] under Grant NRF-2022R1A2C2004874; in part by the Human Resources Development of the Korea Institute of Energy Technology Evaluation and Planning (KETEP) funded by the Korean Government Ministry of Trade, Industry and Energy under Grant 20204030200090; and in part by the Korea Institute of Energy Technology Evaluation and Planning (KETEP) and the Ministry of Trade, Industry & Energy (MOTIE) of the Republic of Korea under Grant 20214000000280.

ABSTRACT Majority of the contemporary hierarchical control strategies for microgrids are either centralized or distributed, relying on leader-follower (or master-slave) consensus for secondary frequency and/or voltage regulation. Thus, in either case, these strategies are susceptible to single-point-failure (SPF). This potential research gap motivated the authors to propose a distributed three-layered hierarchical control strategy applicable to droop-controlled islanded AC microgrids. The proposed strategy can simultaneously ensure (i) frequency and voltage regulation of DGs within the prescribed frequency and voltage deviation limits as per IEC 60034-1 standard (i.e., $\pm 2\%$ and $\pm 5\%$, respectively) without relying on leader-follower consensus at the secondary level, (ii) distributed economic dispatch of active power with minimum error, and (iii) distributed reactive power dispatch with plausible error. The proposed technique is fully distributed and shares the computation and communication burden among the neighboring nodes using a sparse communication network, thus, it is insusceptible to SPF. The feasibility of the proposed technique is guaranteed through various time-domain based numerical simulations executed in Matlab/Simulink under different loading conditions and microgrid expansion.

INDEX TERMS Distributed, dispatch, hierarchical control, leaderless, sliding mode control.

I. INTRODUCTION

The US Department of Energy considers microgrid as the basic building block of a smart grid [1] that incorporates distributed generators (DGs), energy storage systems (ESSs), different loads, and sophisticated control systems [2], [3]. The microgrid can interact with the utility grid in the grid-connected mode, where it behaves as a single controllable unit. However, it can also be operated in the islanded mode, where it behaves as a self-sufficient autonomous power system. A proper control is required for microgrid operation in each mode [4], which refers to a set of decision-making software and/or hardware [5]. Generally, a microgrid control consists of a three-layered hierarchical structure, where the three layers (i.e., primary, secondary, and tertiary) are identified by different communication bandwidths, response times, and execution times [4], [6]–[13]. In the grid-connected mode, both the frequency and voltage are imposed by the utility grid due to its large rotating inertia (rendered by the synchronous generators), thus restricting the microgrid role to perform only the ancillary services [10], [11], [13]–[16]. Conversely, the microgrid control in the autonomous mode is essential for frequency and voltage stability, proper load sharing and reliable power delivery [16].

The primary control is generally enforced as a decentralized (or local) droop controller at each DG. The droop

The associate editor coordinating the review of this manuscript and approving it for publication was Shafi K. Khadem.

controller is responsible for active and reactive power sharing at the cost of pre-specified frequency and voltage deviations, respectively. The secondary layer is responsible for mitigating the frequency and voltage deviations introduced by the primary layer. The tertiary layer is responsible for power flow optimization and cost-effective (i.e., economic) operation of the microgrid [10], [11], [13], [14], [17], [18].

The secondary layer can be implemented as a (i) traditional centralized controller, or (ii) decentralized controller, and (iii) distributed controller. The centralized secondary controller requires a central computation unit and a complex communication network for accessing entire network information. Thus, it bears higher cost and heavy computation burden. It is highly sensitive to failures; thus, it is unreliable and may ultimately lead to to the single-point-failure (SPF) [11], [19]. The decentralized secondary controller also bears higher cost as well as higher reliability [19]. The distributed secondary controller requires a sparse communication network for communication among (local controllers of) neighboring DGs. Thus, it is more reliable, bears lower cost, less sensitive to failures and obviates the requirement of a central computation and communication unit [11], [19]. For a more detailed comparison of various secondary control strategies, the readers are referred to [12], [13]. Traditionally, the tertiary layer can also be implemented as a centralized controller [15] and is susceptible to the same issues stated with reference to the centralized secondary controller.

The main obligation of the hierarchical control of a microgrid is to render control over the generation of power from various DGs [13]. After carrying out an extensive literature review, it has been learn that most of the distributed hierarchical control schemes (despite providing better alternatives to centralized hierarchical control schemes), require a leader (or master) node (or agent) at the secondary level for frequency and/or voltage restoration. This leader agent has to organize and command the operation of its follower (or slave) nodes. Hence, such distributed hierarchical control schemes are again susceptible to the SPF in case of leader outage [20].

Table 1 summarizes the main contributions, features and limitations of the contemporary hierarchical control schemes and the proposed solution.

A. MOTIVATION AND MAJOR CONTRIBUTIONS

The potential research gaps identified in the contemporary hierarchical control schemes for microgrids reported in [21]–[36], and listed in Table 1, motivated the authors to propose a fully distributed hierarchical control strategy applicable to droop-controlled islanded AC microgrids.

The major accomplishments of this article are described below:

1) Distributed secondary frequency and voltage regulation, without requiring any leader-follower (or master-slave) consensus, thus making it a more viable option than the centralized as well as those distributed hierarchical control schemes that are dependent on leader-follower consensus for frequency and/or voltage regulation.
2) Distributed economic dispatch of active power with minimum error.
3) Distributed reactive power dispatch with plausible error.

The performance and effectiveness of the proposed scheme is analyzed and evaluated through time-domain based numerical simulations executed in Matlab/Simulink under different loading conditions and microgrid expansion. It is observed that the proposed scheme successfully fulfills its assigned tasks.

Remark 1: This work is the extension of the authors' previous work reported in [37] focused on three-layered distributed hierarchical control paradigm for frequency restoration and economic dispatch of active power, applicable to droop-controlled islanded AC microgrids. Note that the voltage and reactive power controls had been disregarded in the previous work.

Hence, to further the previous work, the authors have integrated it with the distributed secondary voltage and reactive power control. Moreover, scalability test is performed to demonstrate that the proposed strategy is also applicable to a large AC microgrid system.

The rest of the paper is structured as follows: the communication between energy nodes of the microgrid is explained in Section II using graph theory. The configuration of the microgrid testbench is described in Section III. The detailed closed-loop enforcement of the proposed control strategy is explained in Section IV. Section V gives the performance analysis and effectiveness of the proposed scheme using time-domain based numerical simulations executed in Matlab/Simulink. Finally, Section VI presents concluding remarks to this paper.

II. GRAPH THEORY

In distributed control of microgrids, an energy node (or DG) is considered as an agent. Hence, their mutual interaction can be mathematically and graphically described using the multi-agent system theory. Such that, the communication network interconnecting various agents is represented by a weighted graph, $\mathcal{G}$, which is an ordered pair, $(\mathcal{V}(\mathcal{G}), \mathcal{E}(\mathcal{G}))$, comprising a set of vertices, $\mathcal{V}(\mathcal{G})$, and a set of edges (or arrows or arcs), $\mathcal{E}(\mathcal{G})$, disjoint from the set $\mathcal{V}(\mathcal{G})$. The vertices of the graph indicate the agents, whereas the edges indicate the communication lines (one-way or two-way), which implies that the graph can be directed (one-way) or undirected (two-way). The elements of set $\mathcal{E}(\mathcal{G})$ are indicated as $(\mathcal{V}_i(\mathcal{G}), \mathcal{V}_j(\mathcal{G}))$, implying an edge (or allowed flow of information) from ith to jth agent. Associated with each edge, $(\mathcal{V}_j(\mathcal{G}), \mathcal{V}_i(\mathcal{G})) \in \mathcal{E}(\mathcal{G})$, there is a weight, $a_{ij} \geq 0$, such that $a_{ij} > 0$, for all $(\mathcal{V}_j(\mathcal{G}), \mathcal{V}_i(\mathcal{G})) \in \mathcal{E}(\mathcal{G})$, or if there exists an arrow from jth to ith agent; otherwise $a_{ij} = 0$, for all $i \neq j$, and $i, j = \{1, 2, \ldots, N\}$.

Now, suppose $\mathcal{G} = (\mathcal{V}(\mathcal{G}), \mathcal{E}(\mathcal{G}))$, represents a weighted undirected (two-way) graph, with the set of vertices

TABLE 1. Main contributions, features and limitations of the contemporary hierarchical control schemes and the proposed solution.

Ref.No.	Year	Frequency Regulation	Voltage Regulation	Optimal Dispatch	Limitations/Features
[21]	2016	✓	✗	✗	☞ MGCC[1] is required for dynamic stability, which is prone to SPF. Moreover, voltage regulation and optimal dispatch are neglected.
[22]	2017	✓	✓	✗	☞ A centralized MPC based supervisory control scheme is required, which is prone to SPF[2].
[23]	2018	✓	✓	✓	☞ Leader-follower consensus is required for the distributed secondary frequency and voltage control, which is prone to SPF.
[24]	2018	✓	✓	✗	☞ Leader-follower consensus is required for the distributed secondary frequency and voltage control, which is prone to SPF. Also, optimal dispatch is neglected.
[25]	2019	✓	✗	✓	☞ It does not consider secondary voltage regulation for AC microgrid subsystem. Moreover, only active loads and, hence, active power flow have been considered. Hence, there is no reactive power flow in the AC microgrid subsystem. The tertiary controller in the upper control layer is centralized and, hence, prone to SPF.
[26]	2019	✓	✗	✓	☞ Only active power is dispatched. Voltage regulation and reactive power dispatch are neglected. Generation cost parameters have not been considered. Moreover, the power lines are assumed to be loss-less (purely inductive).
[27]	2020	✓	✓	✓	☞ MGCC is required for optimal dispatch, voltage and synchronization control, which is prone to SPF.
[28]	2020	✗	✓	✓	☞ Only reactive power is dispatched. Frequency regulation and active power dispatch are neglected.
[29]	2020	✓	✗	✓	☞ Only active power is dispatched. Voltage regulation and reactive power dispatch are neglected.
[30]	2020	✓	✗	✓	☞ Only active power is dispatched. Voltage regulation and reactive power dispatch are neglected. Generation cost parameters have not been considered. Moreover, the power lines are assumed to be loss-less (purely inductive).
[31]	2021	✓	✗	✓	☞ Only active power is dispatched. Voltage regulation and reactive power dispatch are neglected. Generation cost parameters have not been considered. Moreover, the power lines are assumed to be loss-less (purely inductive).
[32]	2021	✓	✗	✓	☞ Only active power is dispatched. Voltage regulation and reactive power dispatch are neglected. Generation cost parameters have not been considered. Moreover, the power lines are assumed to be loss-less (purely inductive).
[33]	2021	✓	✓	✓	☞ Leader-follower consensus is required for the distributed secondary frequency and voltage control, which is prone to SPF. Moreover, the optimal dispatch is focused on the minimization of overall network power losses only, and generation cost minimization has been neglected.
[34]	2021	✓	✗	✓	☞ It does not consider secondary voltage regulation for AC microgrid subsystem. Moreover, only active loads and, hence, active power flow have been considered. Hence, there is no reactive power flow in the AC microgrid subsystem.
[35]	2021	✗	✓	✗	☞ It does not consider frequency regulation and economic active power dispatch.
[36]	2022	✗	✓	✗	☞ It does not consider frequency regulation and economic active power dispatch.
Proposed	2022	✓	✓	✓	☞ Leader-follower consensus is not required for the distributed secondary frequency and voltage control, hence, it is insusceptible to SPF. Moreover, both active and reactive powers are dispatched.

[1] MGCC = Microgrid Central Controller
[2] SPF = Single-Point-Failure

$\mathcal{V}(\mathcal{G}) = \{\mathcal{V}_1(\mathcal{G}),\ \mathcal{V}_2(\mathcal{G}),\ \ldots,\ \mathcal{V}_N(\mathcal{G})\}$, and the set of edges $\mathcal{E}(\mathcal{G}) \subset \mathcal{V} \times \mathcal{V}$. Then, the graph structure and properties can be described by inspecting the properties of few associated matrices, that is, the weighted adjacency matrix, $\mathcal{A} = [a_{ij}] \in R^{N\times N}$, the weighted in-degree matrix, $\mathcal{D}^{in} = diag\{d_i^{in}\} \in R^{N\times N}$ where $d_i^{in} = \sum_{j\in\mathcal{N}_i} a_{ij}$, and the weighted Laplacian matrix, $\mathcal{L} = \mathcal{D}^{in} - \mathcal{A} \in R^{N\times N}$, where N indicates the number of agents. Let $\mathcal{N}_i$ and $|\mathcal{N}_i|$, respectively, indicate the neighboring agents set of ith agent, and the number of (in-) neighbors of ith agent, then $\mathcal{N}_i = \{\mathcal{V}_j : (\mathcal{V}_j, \mathcal{V}_i) \in \mathcal{E}\}$, and $|\mathcal{N}_i| = d_i^{in}$, that is, the in-degree of ith agent [38], [39].

III. TESTBENCH CONFIGURATION

The correctness and soundness of the proposed idea is validated in Matlab/Simulink using a three-phase microgrid simulation testbench, which is shown in Fig. 1. This testbench consists of three DGs, four buses, various (resistive and reactive/inductive) loads, and interconnecting lines. Note that two out of three DGs are low-inertia type (i.e., inverter-interfaced), while the third DG is high-inertia type (i.e., rotating type synchronous-generator based diesel genset). The inverter-interfaced DGs (i.e., DG1 and DG2) are connected to bus 1 and 3, while the diesel genset (i.e., DG3) is connected to bus 4 through three-phase ΔY-transformers. The line impedances between the four buses (i.e., Z_{12}, Z_{13}, Z_{24} and Z_{34}) represent RLC-branches. Moreover, two out of three remaining impedances between DGs and transformers, that is, Z_1 and Z_2, indicate coupling inductances, while Z_3 indicates a coupling capacitor. Tables 2–5, describe various parameters of the simulation testbench, shown in Fig. 1.

IV. PROPOSED THREE-LAYERED DISTRIBUTED HIERARCHICAL CONTROL SCHEME

Figure 2 demonstrates the closed-loop enforcement of the formulated three-layered distributed hierarchical control scheme. The primary layer is based on the droop control,

TABLE 2. Microgrid testbench transformers specifications.

TAG	Rating (kVA)	Frequency (Hz)	Primary Winding Specifications			Secondary Winding Specifications		
			V_{ph-ph} (V)	R (Ω)	X_L (Ω)	V_{ph-ph} (V)	R (Ω)	X_L (Ω)
T_1	45	60	208	0.02688	0.1075	208	0.005047	0.0201
T_2	45	60	208	0.02688	0.1075	208	0.005047	0.0201
T_3	45	60	208	0.02688	0.1075	208	0.005047	0.0201

TABLE 3. Microgrid testbench impedances specifications.

Line Impedances	R (Ω)	X_L (Ω)	X_C (Ω)
Z_1	0	1.884	0
Z_2	0	1.884	0
Z_3	0	0	26.53
Z_{12}	0.027352	0.0066	288.60
Z_{13}	0.0137	0.0033	577.20
Z_{24}	0.01688	0.00407	336.70
Z_{34}	0.0026	0.00064	2020.10

TABLE 4. Inverter-based DGs specifications.

DG1 and DG2 Specifications	
Quantity	Value
S_{base}	15 kVA
V_{base}	208 V
V_{DC}	750 V
f_{ref}	60 Hz
Δf	0.50 Hz
ω_{ref}	377 rad s^{-1}
$\Delta\omega$	π rad s^{-1}
P_{max}	15 kW or 1 pu
P_{min}	0 kW
V_{ref}	208 V or 1 pu
$K_{P,p}$	3
$K_{P,i}$	30
$K_{V,p}$	0.01
$K_{V,i}$	5
κ_P	π
κ_Q	0.05
τ_V, τ_P, τ_Q	0.01 s
Z_{vir}	11.856 mH

TABLE 5. ICE-based diesel genset (i.e., DG3) specifications.

DG3 Specifications			
Quantity	Value	Quantity	Value
S_{base}	12.50 kVA	X_q	0.53301
V_{base}	208 V	X''_q	0.051
f_{ref}	60 Hz	X_l	0.037
Δf	0.50 Hz	T'_d	0.35523
ω_{ref}	377 rad s^{-1}	T''_d	0.00015
$\Delta\omega$	π rad s^{-1}	T''_q	0.0067
P_{max}	12.50 kW or 1 pu	R_s	0.0217 pu
P_{min}	0 kW	$H(s)$	0.1901
V_{ref}	208 V or 1 pu	p	2
$K_{P,p}$	3	$K_{G,p}$	10
$K_{P,i}$	30	$K_{G,i}$	20
$K_{V,p}$	1000	K_{tf}	0.625
$K_{V,i}$	10	K_{ev}	11.8238
κ_P	π	K_{fv}	3600
κ_Q	0.05	η_{th}	0.47
τ_V, τ_P, τ_Q	0.01 s	τ_d	0.022 s
X_d	1.204	K_m	0.36
X'_d	0.125	τ_{ex}	0.001 s
X''_d	0.056	Z_{vir}	11.856 mH

the secondary level is enforced as the distributed secondary active power/frequency and voltage/reactive power control

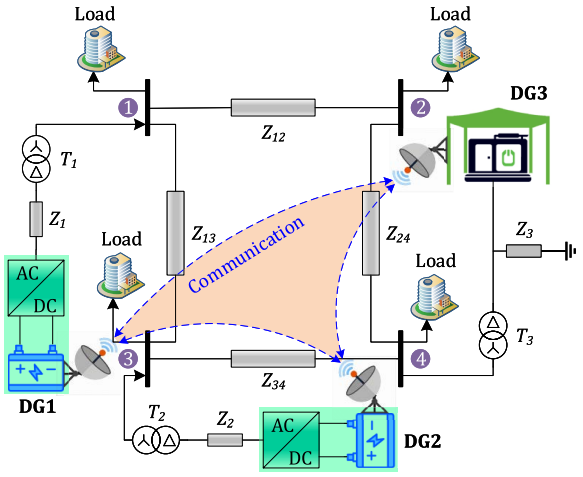

FIGURE 1. Microgrid simulation testbench.

without requiring any leader-follower consensus, and the tertiary layer is based on the distributed economic dispatch of active power.

A. PRIMARY CONTROL

The primary control is provided at each DG using the conventional droop technique. It consists of $P\omega$- and QV-droop controls that are, respectively, expressed in (1) below [40], [41]:

$$\left.\begin{aligned} \omega_i &= \omega_{ref} + \Delta\omega_{i,adj} + \kappa_{i,P}\left(P_{i,set} - P_i\right) \\ V_{i,pk} &= V_{i,set} + I_{i,RMS}Z_{vir} - V_i - \kappa_{i,Q}Q_i \end{aligned}\right\} \quad (1)$$

where the subscript $i = \{1, 2, \ldots, N = 3\}$ denotes the DGs index set, ω_i is the ith DG frequency, ω_{ref} is the microgrid reference frequency (i.e., 60 Hz), $\Delta\omega_{i,adj}$ is the ith DG frequency adjustment factor provided by the overload control strategy, as reported in [42], $\kappa_{i,P} > 0$ represents the ith DG $P\omega$-droop control gain, $P_{i,set}$ is the ith DG active power set-point, and P_i is the ith DG active power output. Note that the active power set-point, $P_{i,set}$, is provided by the distributed secondary active power controller, expressed in (4), to the primary (i.e., $P\omega$-droop) controller. Furthermore, V_i is the ith DG output voltage, $V_{i,set}$ is the ith DG voltage set-point, $I_{i,RMS}Z_{vir}$ is the voltage drop due to the (inductive) virtual impedance, $\kappa_{i,Q} > 0$ is the ith DG QV-droop control (adjustable) gain, and Q_i represents the ith DG output reactive power. In case of inverter-based DGs, $V_{i,pk}$ indicates the peak voltage at the inverter terminals, whereas for genset $V_{i,pk} = V_{cmd}$ represents the input voltage command to the field-exciter control block of the synchronous generator for generating field excitation, V_f. Note that the voltage set-point, $V_{i,set}$, is provided by the distributed secondary voltage control

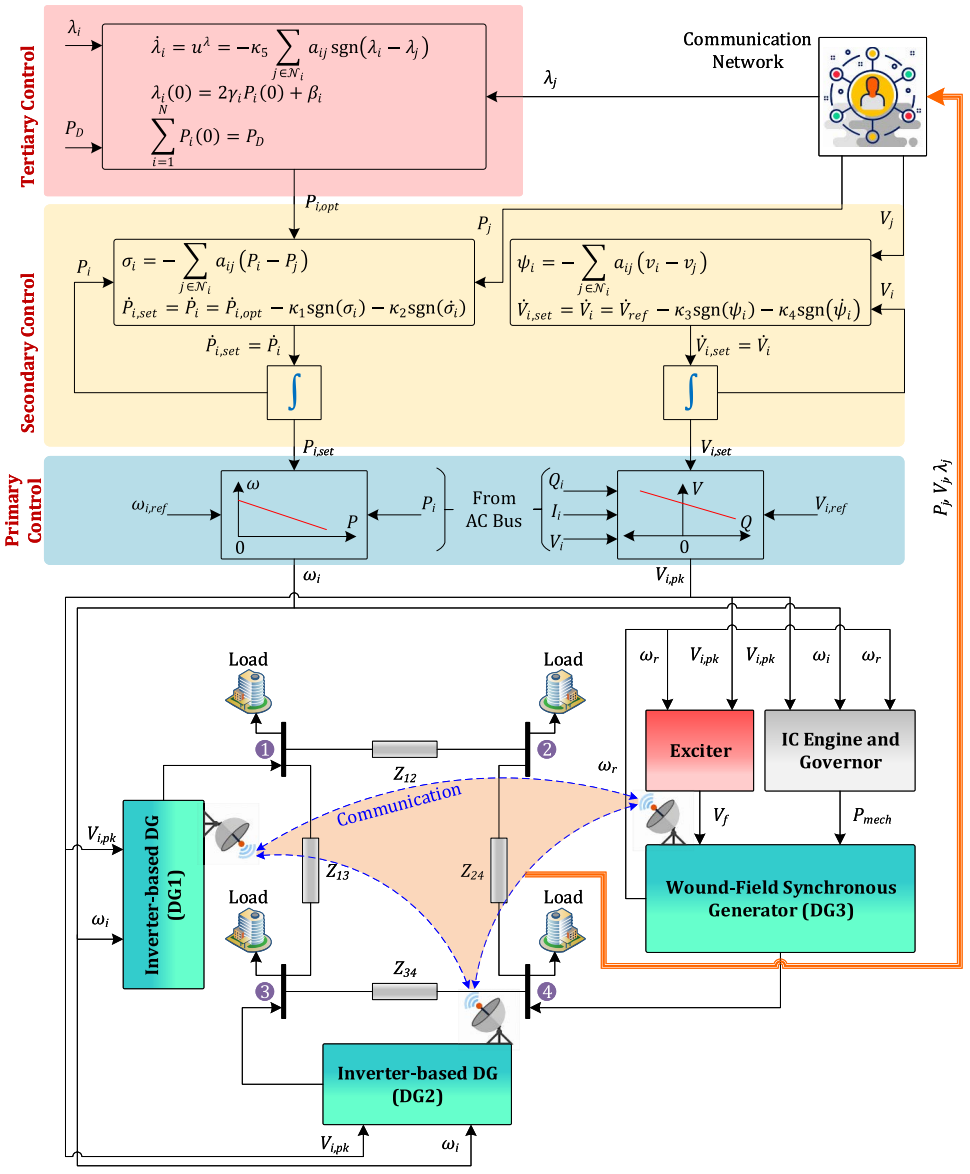

FIGURE 2. Overall enforcement of the formulated three-layered distributed hierarchical control paradigm.

algorithm, expressed in (7), to the primary (or QV-droop) controller, given in (1).

The two inverter-interfaced DGs (i.e., DG1 and DG2) are mimicked as three-phase controlled AC voltage sources, where the instantaneous voltages for each phase (i.e., v_a, v_b and v_c), as depicted in Fig. 3, are given in (2) below [37]:

$$\left.\begin{aligned} v_a &= V_{i,pk}\sin(\omega_i t + 0^\circ) \\ v_b &= V_{i,pk}\sin(\omega_i t - 120^\circ) \\ v_c &= V_{i,pk}\sin(\omega_i t + 120^\circ) \end{aligned}\right\} \tag{2}$$

where $V_{i,pk}$ equals the product of the modulation index, M_D, and the inverter DC input voltage, V_{DC} (i.e., $V_{i,pk} = M_D V_{DC}$).

For inverter-interfaced DGs and genset, the primary controls are shown in Figs. 3 and 4, respectively. The corresponding simulation parameters for each are, respectively, specified in Tables 4 and 5. Let F_{cmd}, T_{cmd}, T_F, F_p, ω_r, and P_{fr}, respectively, indicate the fuel command, torque command, fuel toque, fuel power, rotational speed of synchronous generator, and friction power losses for genset, as shown in Fig. 4, then

$$\left.\begin{aligned} F_{cmd} &= K_{tf} T_{cmd} \\ T_F &= \eta_{th} K_{fv} K_{ev} F_{cmd} \\ F_p &= T_F \omega_r \\ P_{fr} &= K_m \omega_r^2 \end{aligned}\right\} \tag{3}$$

where (K_{tf}, η_{th}, K_{fv}, K_{ev} and K_m) > 0 are constants, specified in Table 5.

B. SECONDARY CONTROL

The secondary control is provided at each DG using the distributed technique that concurrently ensures:

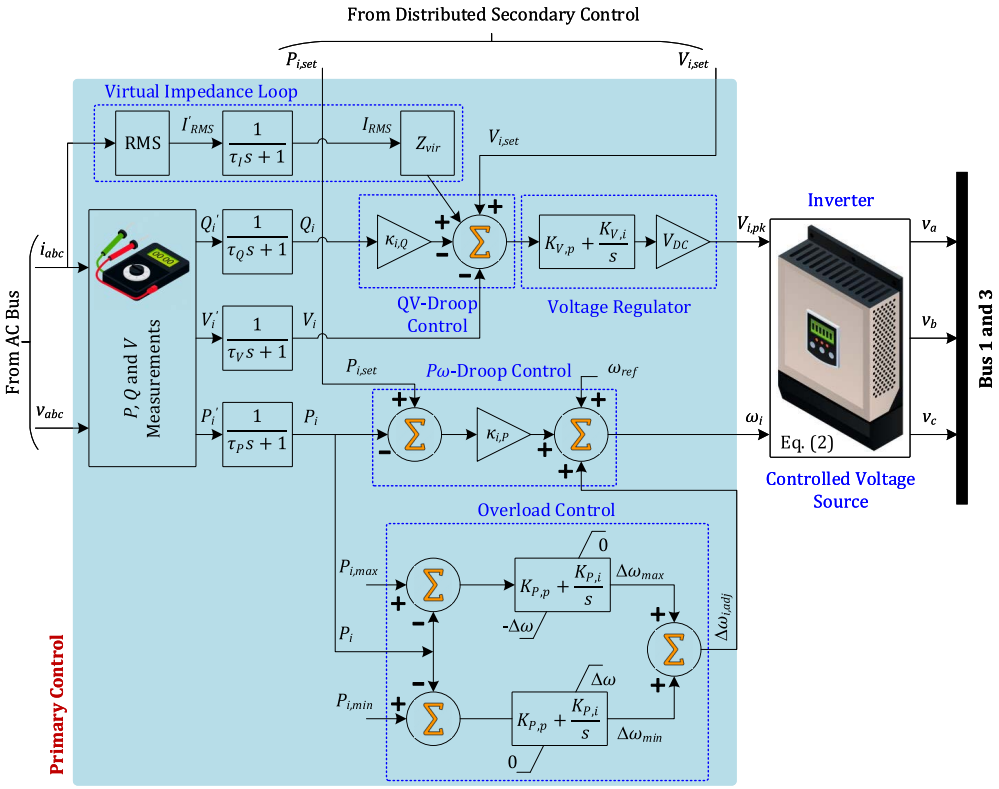

FIGURE 3. Droop-based primary control enforcement for DG1 and DG2 (i.e., inverter-interfaced DGs).

1) Active power control and frequency restoration of DGs in a finite-time, without requiring any devoted supplementary frequency control, and compensates for frequency deviation under load perturbation, and
2) Voltage and reactive power control of DGs in a finite-time.

1) ACTIVE POWER AND FREQUENCY CONTROL

Inspired by [43], [44], the above-stated objective (1) (i.e., active power and frequency control) is achieved by formulating the following higher-order twisting sliding mode based distributed secondary active power tracking control algorithm:

$$\left.\begin{aligned}&\text{if } \sigma_i(t) = -\sum_{j\in\mathcal{N}_i} a_{ij}\big(P_i(t)-P_j(t)\big)\\&\text{then } \dot{z}_{pi}(t) = u_i^P(t) = -\kappa_1\,\mathrm{sgn}\big(\sigma_i(t)\big) - \kappa_2\,\mathrm{sgn}\big(\dot{\sigma}_i(t)\big)\\&\text{and } P_{i,set}(t) = P_i = z_{pi}(t) + r_{pi}(t) = z_{pi}(t) + P_{i,opt}(t)\end{aligned}\right\} \tag{4}$$

so that

$$\left.\begin{aligned}&\big\|P_i(t) - P_{i,opt}(t)\big\| \to 0\\&\Big\|\sum_{i=1}^{N} P_i(t) - P_D(t)\Big\| \to 0\\&\big\|\omega_i(t) - \omega_{ref}\big\| \to 0\end{aligned}\right\}, \quad \text{as } t\to\infty$$

where σ_i is the active power error between the neighboring agents, $a_{ij} \geq 0$ is the ijth elements of the adjacency matrix, A, $z_{pi} \in \mathbb{R}^N$ is an auxiliary (or intermediate) state variable for active power control, u_i^P is the twisting-based sliding mode control law for active power, $\kappa_1,\ \kappa_2 > 0$ are the adjustable design parameters (where $\kappa_1 > \kappa_2$), sgn is the multi-valued signum function, $r_{pi}(t) = P_{i,opt} \in \mathbb{R}^N$ is a time-varying signal indicating the optimal active power dispatch reference (with a bounded derivative), which is generated and provided by the distributed tertiary controller, expressed in (17), to the distributed secondary active power controller, described in (4), while P_D represents the combined active power demand.

The auxiliary state variable, z_{pi}, in (4), is initialized such that:

$$\left.\begin{aligned}&z_{pi}(0) = 0\\&\sum_{i=1}^{N} z_{pi}(0) = 0\end{aligned}\right\} \tag{5}$$

Taking time-derivative of $P_{i,set}$ in (4), the following closed-loop system is obtained:

$$\left.\begin{aligned}\dot{P}_{i,set}(t) &= \dot{P}_i(t)\\&= \dot{z}_{pi}(t) + \dot{P}_{i,opt}(t)\\&= \dot{P}_{i,opt}(t) - \kappa_1\,\mathrm{sgn}\big(\sigma_i(t)\big) - \kappa_2\,\mathrm{sgn}\big(\dot{\sigma}_i(t)\big)\end{aligned}\right\} \tag{6}$$

where the initial conditions are: $\sum_{i=1}^{N} P_i(0) = \sum_{i=1}^{N} P_{i,opt}(0)$.

In (6), $P_{i,set}$ indicates the active power reference signal generated by the distributed secondary active power controller and provided to the $P\omega$-droop primary controller,

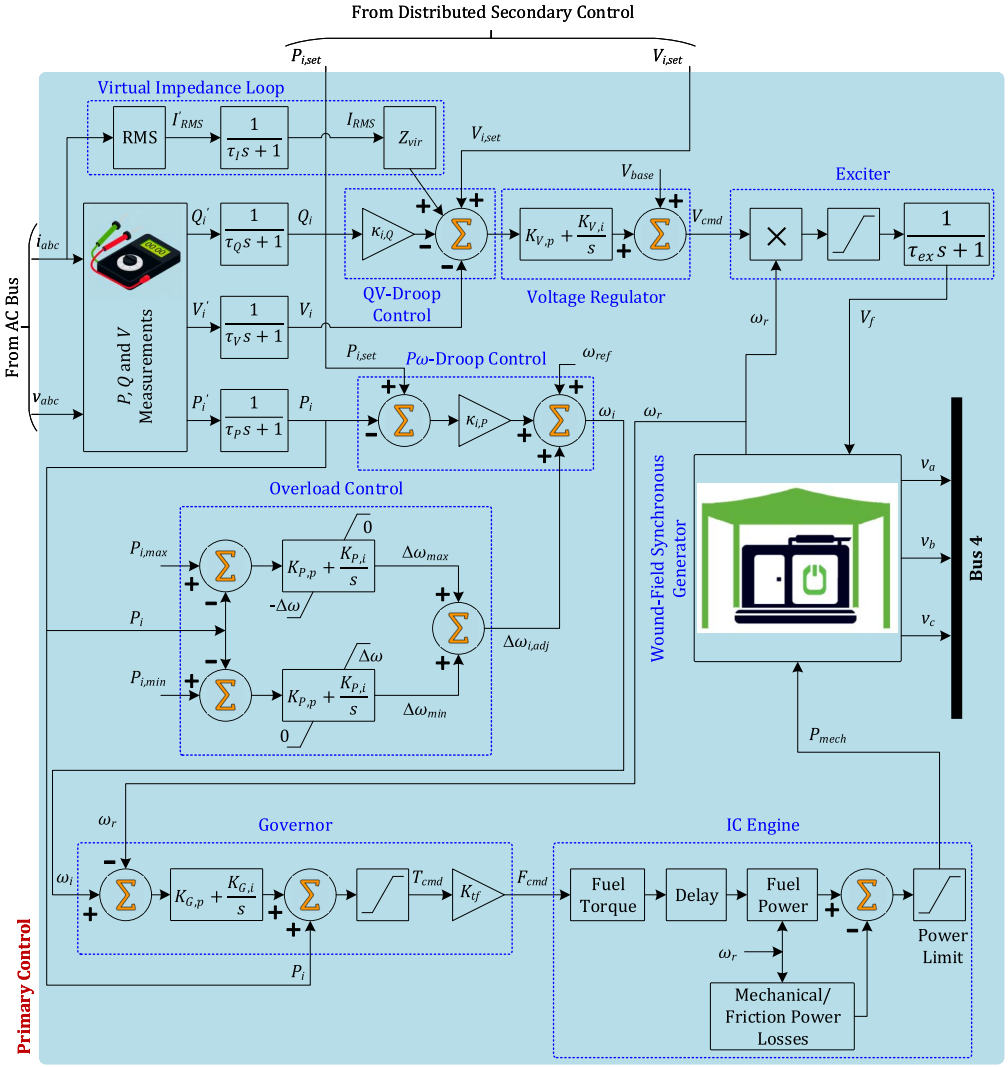

FIGURE 4. Droop-based primary control enforcement for DG3 (i.e., ICE-interfaced diesel genset).

expressed in (1). The enforcement of the distributed secondary active power controller is shown in Fig. 2.

The principal roles of the distributed secondary active power tracking control algorithm, given in (4), are as follows:

1) To force each agent (i.e., DG) of the microgrid to track its corresponding time-varying reference signal (i.e., the optimal active power dispatch reference, $P_{i,opt}$) provided by the distributed tertiary controller with a negligible active power mismatch (i.e., $\Delta P = \| \sum_{i=1}^{N} P_i - P_D \| \cong 0$)
2) To, concurrently, ensure the frequency restoration of each agent to the reference frequency, ω_{ref}, without requiring any dedicated auxiliary frequency control.

2) VOLTAGE AND REACTIVE POWER CONTROL

Similarly, the stated objective (2) (i.e., voltage and reactive power control), described in Section IV.B, is achieved by formulating the following higher-order twisting sliding mode based distributed secondary voltage tracking control algorithm:

$$\left.\begin{aligned} &\text{if } \psi_i(t) = -\sum_{j\in\mathcal{N}_i} a_{ij}\left(V_i(t) - V_j(t)\right) \\ &\text{then } \dot{z}_{vi}(t) = u_i^V(t) = -\kappa_3\,\mathrm{sgn}\big(\psi_i(t)\big) - \kappa_4\,\mathrm{sgn}\big(\dot{\psi}_i(t)\big) \\ &\text{and } V_{i,set}(t) = V_i(t) = z_{vi}(t) + r_{vi}(t) = z_{vi}(t) + V_{ref} \end{aligned}\right\} \tag{7}$$

so that

$$\left.\begin{aligned} &\left\| V_i(t) - V_j(t) \right\| \to 0 \\ &\left\| V_i(t)(t) - V_{ref} \right\| \to 0 \\ &\left\| \sum_{i=1}^{N} Q_i(t) - Q_D(t) \right\| \to 0 \end{aligned}\right\}, \quad \text{as } t \to \infty$$

where ψ_i is the voltage error between the neighboring agents, $z_{vi} \in \mathbb{R}^N$ is an auxiliary state variable for secondary voltage control, u_i^V is the twisting-based sliding mode control law for voltage, $\kappa_3,\ \kappa_4 > 0$ are tunable design parameters

(where $\kappa_3 > \kappa_4$), $r_{vi}(t) = V_{ref} \in \mathbb{R}^N$ is the local input reference voltage signal (with a bounded derivative), and Q_D is the total reactive power demand.

The auxiliary state variable, z_{vi}, in (7), is initialized such that:

$$\left.\begin{aligned} z_{vi}(0) &= 0 \\ \sum_{i=1}^{N} z_{vi}(0) &= 0 \end{aligned}\right\} \tag{8}$$

Taking time-derivative of $V_{i,set}$ in (7), the following closed-loop system is obtained:

$$\left.\begin{aligned} \dot{V}_{i,set}(t) &= \dot{V}_i(t) \\ &= \dot{z}_{vi}(t) + \dot{V}_{ref} \\ &= \dot{V}_{ref} - \kappa_3 \operatorname{sgn}\big(\psi_i(t)\big) - \kappa_4 \operatorname{sgn}\big(\dot{\psi}_i(t)\big) \end{aligned}\right\} \tag{9}$$

In (9), $V_{i,set}$ indicates the reference voltage signal commanded by the distributed secondary voltage tracking control algorithm to the QV-droop primary controller, expressed in (1). The enforcement of the distributed secondary voltage tracking control algorithm is shown Fig. 2.

The principal roles of the distributed secondary voltage tracking control algorithm, given in (7), are as follows:

1) To force each agent (i.e., DG) of the microgrid to track the local input reference voltage, V_{ref}, and
2) Concurrently, fulfill the reactive power demand, Q_D, with a plausible mismatch (i.e., $\Delta Q = \| \sum_{i=1}^{N} Q_i - Q_D \| \cong 0$.

3) CONVERGENCE ANALYSIS

This section provides the convergence analysis of the distributed secondary active power tracking control algorithm, expressed in (4). Furthermore, it will also serve as a basis for the convergence analysis of the distributed secondary voltage tracking control algorithm, expressed in (7), because it also has the same form.

The discontinuous signum function, appearing in the control algorithm (4), introduces discontinuity in it. Therefore, the solution of the stated control algorithm can be interpreted in the Filippov sense [45].

Lemma 1: Suppose the communication graph, $\mathcal{G}$, is connected and $\|P_i(t) - P_j(t)\| = 0$, for all $i, j = \{1, 2, \ldots, N\}$, then $\|P_i(t) - P_{i,opt}(t)\| = 0$, for all $i = \{1, 2, \ldots, N\}$.

Proof: It follows from (4) that:

$$\sum_{i=1}^{N} P_i(t) = \sum_{i=1}^{N} z_{pi}(t) + \sum_{i=1}^{N} P_{i,opt}(t) \tag{10}$$

Because, the graph, $\mathcal{G}$, shown in Fig. 1, is undirected, it follows that:

$$\sum_{i=1}^{N} \dot{z}_{pi}(t) = \sum_{i=1}^{N} -\kappa_1 \operatorname{sgn}\big(\sigma_i(t)\big) - \kappa_2 \operatorname{sgn}\big(\dot{\sigma}_i(t)\big) = 0 \tag{11}$$

Since $\sum_{i=1}^{N} z_{pi}(0) = 0$ (see (5)), therefore, it follows that $\sum_{i=1}^{N} z_{pi}(t) \equiv 0$ forall $t \geq 0$, which yields,

$$\sum_{i=1}^{N} P_i(t) = \sum_{i=1}^{N} P_{i,opt}(t) \quad \text{for all } t \geq 0 \tag{12}$$

Provided that $\big\|P_i(t) - P_j(t)\big\| = 0$, for all $i, j = \{1, 2, \ldots, N\}$, it follows from (12) that $\big\|P_i(t) - P_{i,opt}(t)\big\| = 0$, for all $i = \{1, 2, \ldots, N\}$. To rephrase it, the distributed secondary active power tracking control algorithm, given in (4), warrants that each $P_i(t)$ tracks its corresponding $P_{i,opt}(t)$, in a finite-time. This completes the proof. □

C. TERTIARY CONTROL

The total generation cost of a system of N generators can be minimized by scheduling each generator's active power output, subject to the system constraints. This task is performed by the tertiary controller, which prescribes the optimal active power dispatch reference, $P_{i,opt}$, for each ith DG, and renders it to the distributed secondary active power tracking control algorithm, stated in (4) and depicted in Fig. 2.

Now, the above-mentioned active power scheduling or the economic load dispatch (ELD) issue may be figured out either in a: (i) centralized, or (ii) distributed mode.

1) CENTRALIZED TERTIARY CONTROL

The ELD problem is conventionally solved by employing a centralized tertiary controller. The objective function is to minimize the total generation cost, subject to the generation-demand equality (or power balance) and inequality (or power generation capacity) constraints, and can be described as follows [46], [47]:

$$\left.\begin{aligned} &\text{Objective function:} \\ &\min \sum_{i=1}^{N} C_i(P_i) = \min \sum_{i=1}^{N} \left(\gamma_i P_i^2 + \beta_i P_i + \alpha_i\right) \\ &\text{s.t.} \\ &\quad \sum_{i=1}^{N} P_i = P_D \quad \text{(equality constraint)} \\ &\quad P_{i,\min} \leq P_i \leq P_{i,\max} \quad \text{(inequality constraint)} \end{aligned}\right\} \tag{13}$$

where $C_i(P_i)$ indicates the generation cost of ith DG approximated by a quadratic type function, $\sum_{i=1}^{N} C_i$ is the total generation cost, α_i, β_i, and $\gamma_i > 0$ are the generation cost coefficients, P_i is the active power output of ith DG with its lower and upper limits, respectively, indicated by $P_{i,\min}$ and $P_{i,\max}$, and P_D represents the total active power demand.

Among several typical approaches for centralized solution of ELD problem, one is the Lagrange multiplier technique. In this stated method, the system constraints are integrated into the objective function. The Lagrangian function, L, for working out the ELD problem can be written as under:

$$L(P_i, \lambda) = \sum_{i=1}^{N} C_i(P_i) + \lambda \left(P_D - \sum_{i=1}^{N} P_i\right) \tag{14}$$

where λ indicates the Lagrange multiplier associated with the power balance constraint, stated in (13).

Then, the first-order Karush-Kuhn-Tucker optimization conditions are applied as under:

$$\left.\begin{aligned}
&\underline{\text{Condition 1 yields:}}\\
&\frac{\partial L}{\partial P_i} = \frac{\partial \sum_{i=1}^{N} C_i(P_i)}{\partial P_i} - \lambda = 0\\
&\Longrightarrow \lambda_{opt} = \frac{dC_i(P_i)}{dP_i} = \beta_i + 2\gamma_i P_{i,opt}\\
&\Longrightarrow P_{i,opt} = \frac{\lambda_{opt} - \beta_i}{2\gamma_i} \geq 0\\
&\underline{\text{Condition 2 yields:}}\\
&\frac{\partial L}{\partial \lambda} = P_D - \sum_{i=1}^{N} P_i = 0\\
&\Longrightarrow \sum_{i=1}^{N} P_{i,opt} = P_D\\
&\Longrightarrow \lambda_{opt} = \frac{P_D + \sum_{i=1}^{N} \frac{\beta_i}{2\gamma_i}}{\sum_{i=1}^{N} \frac{1}{2\gamma i}}
\end{aligned}\right\} \tag{15}$$

Note that (15) identifies the necessary conditions for the ELD problem (i.e., the minimum generation cost). It implies that the ELD problem corresponds to the active power dispatch for which the incremental cost of each generator (i.e., $dC_i(P_i)/dP_i$) equals the Lagrangian multiplier, λ. For this reason, the stated strategy is called the equal incremental cost criterion. However, (15) considers the equality constraints only, and neglects the inequality constraints (i.e., $P_{i,\min} = 0$ and $P_{i,\max} = \infty$).

So, considering the inequality constraint too (i.e., $P_{i,\min} \leq P_i \leq P_{i,\max}$), the optimal power dispatch conditions, given in (15), can be revised as follows:

$$\left.\begin{aligned}
&2\gamma_i P_{i,opt} + \beta_i = \lambda_{opt}, \quad \text{for } P_{i,min} < P_i < P_{i,max}\\
&2\gamma_i P_{i,opt} + \beta_i \leq \lambda_{opt}, \quad \text{for } P_i = P_{i,max}\\
&2\gamma_i P_{i,opt} + \beta_i \geq \lambda_{opt}, \quad \text{for } P_i = P_{i,min}
\end{aligned}\right\} \tag{16}$$

Note that λ_{opt} (i.e., the optimal incremental cost) is calculated using the last expression in (15), and then substituted into (16) to find the $P_{i,opt}$ (i.e., the optimal active power dispatch reference) for each DG. Finally, from the centralized tertiary controller, these stated dispatch references are provided to the distributed secondary active power tracking control algorithm, given in (4).

2) DISTRIBUTED TERTIARY CONTROL

The contemporary approach for solving the ELD problem is to employ a distributed tertiary controller, which can also establish the equal incremental cost criterion by employing consensus control algorithms.

Motivated by [48], the following finite-time incremental cost consensus control algorithm is proposed to find a distributed solution to the ELD problem:

$$\left.\begin{aligned}
&\dot{\lambda}_i(t) = u_i^{\lambda}(t) = -\kappa_5 \sum_{j \in \mathcal{N}_i} a_{ij} \operatorname{sgn}\left(\lambda_i(t) - \lambda_j(t)\right)^c\\
&\text{s.t. } \lambda_i(0) = \beta_i + 2\gamma_i P_i(0)\\
&\sum_{i=1}^{N} P_i(0) = P_D
\end{aligned}\right\} \tag{17}$$

where u_i^{λ} denotes the distributed tertiary control law for the incremental cost consensus, $\kappa_5 > 0$, and $0 < c < 1$ are the adjustable design parameters, and $\operatorname{sgn}(\cdot)^c = \operatorname{sgn}(\cdot)|\cdot|^c$.

3) CONVERGENCE ANALYSIS

This section provides the convergence analysis of the distributed tertiary controller, described in (17). For this purpose, some Lemmas are needed, as given below:

Lemma 2: Let $b_1, b_2, \ldots, b_n \geq 0$ and $(0 < r < p)$, then [49]

$$\left(\sum_{i=1}^{N} b_i^p\right)^{1/p} \leq \left(\sum_{i=1}^{N} b_i^r\right)^{1/r}$$

Lemma 3: Let $\Im_2(L)$ denotes the second smallest positive eigenvalue of the Laplacian matrix, L, $\mathbf{1}^T x = 0$, and the communication graph, $\mathcal{G}$, be undirected, the matrix L possesses the following properties [50]:

1) $x^T L x \geq \Im_2(L) x^T x$

2) $x^T L x = \frac{1}{2} \sum_{i,j=1}^{N} a_{ij} \left(x_i - x_j\right)^2$. Moreover, the matrix L is positive semi-definite.

Lemma 4: Suppose $V(x) : \mathbb{R}^N \to \mathbb{R}$, be a C-regular function. Furthermore, $x(t) : [0, +\infty) \to \mathbb{R}^N$ be an absolutely continuous function on any compact time-interval of $[0, +\infty)$, and the following inequality is satisfied:

$$\frac{dV(t)}{dt} \leq -KV^m(t)$$

where $K > 0$ and $(0 < m < 1)$. Then $V(t) = 0$ for all $t \geq t_s$, and the settling time, t_s, can be estimated by [51]:

$$t_s = \frac{V^{1-m}(0)}{K(1-m)}$$

Proof: Having Lemmas 2 through 4, it is now easy to understand the convergence of the distributed tertiary control law.

Suppose $\delta_i(t) = \{\delta_1(t), \delta_2(t), \ldots, \delta_N(t)\}$ be the incremental cost consensus error of *i*th DG, described as under:

$$\delta_i(t) = \lambda_i(t) - \frac{1}{N} \sum_{i=1}^{N} \lambda_i(t) \tag{18}$$

Since, $\frac{1}{N} \sum_{i=1}^{N} \lambda_i(t)$ is time-invariant (i.e., a constant average value), therefore, $\frac{1}{N} \sum_{i=1}^{N} \dot{\lambda}_i(t) = 0$ for a connected and undirected communication graph, $\mathcal{G}$.

Now, using $\text{sgn}(\cdot)^c = \text{sgn}(\cdot)|\cdot|^c$, the differential error for (18), $\dot{\delta}(t)$, can be expressed as follows:

$$\left.\begin{aligned}\dot{\delta}_i(t) &= \dot{\lambda}_i(t) - \frac{1}{N}\sum_{i=1}^{N}\cancelto{0}{\dot{\lambda}_i(t)} \\ &= \kappa_5 \sum_{j\in\mathcal{N}_i} a_{ij}\,\text{sgn}\left(\lambda_j(t)-\lambda_i(t)\right)\left|\lambda_j-\lambda_i\right|^c \\ &= \kappa_5 \sum_{j\in\mathcal{N}_i} a_{ij}\,\text{sgn}\left(\delta_j-\delta_i\right)\left|\delta_j-\delta_i\right|^c\end{aligned}\right\} \tag{19}$$

Let, V_λ be the Lyapunov function candidate, such that

$$V_\lambda = 2\Im_2\delta^T(t)\delta(t) = 2\Im_2\sum_{i=1}^{N}\delta_i^2(t) \tag{20}$$

Let an undirected graph, $\mathcal{G}_\lambda$, has an associated adjacency matrix, $A_\lambda = [a_{\lambda ij}]_{N\times N} = [(\kappa_5 a_{ij})^{\frac{2}{1+c}}]_{N\times N}$, a Laplacian matrix, L_λ, and $\Im_{2\lambda}$ as the second smallest positive eigenvalue of the Laplacian matrix, L_λ. Thus, the time-derivative of V_λ can be described as:

$$\left.\begin{aligned}\dot{V}_\lambda &= 4\Im_2\sum_{i=1}^{N}\delta_i(t)\dot{\delta}_i(t) \\ &= 4\Im_2\sum_{i=1}^{N}\delta_i \\ &\left[\sum_{j\in\mathcal{N}_i} a_{\lambda ij}^{\frac{1+c}{2}}\,\text{sgn}\left(\delta_j-\delta_i\right)\left|\delta_j-\delta_i\right|^c\right] \\ &= 2\Im_2\sum_{i,j=1}^{N} a_{\lambda ij}^{\frac{1+c}{2}}\,\delta_i\,\text{sgn}\left(\delta_j-\delta_i\right)\left|\delta_j-\delta_i\right|^c \\ &\quad + 2\Im_2\sum_{i,j=1}^{N} a_{\lambda ji}^{\frac{1+c}{2}}\,\delta_j\,\text{sgn}\left(\delta_i-\delta_j\right)\left|\delta_i-\delta_j\right|^c \\ &= 2\Im_2\sum_{i,j=1}^{N} a_{\lambda ij}^{\frac{1+c}{2}}\left(\delta_i-\delta_j\right)\text{sgn}\left(\delta_j-\delta_i\right)\left|\delta_j-\delta_i\right|^c \\ &= -2\Im_2\sum_{i,j=1}^{N} a_{\lambda ij}^{\frac{1+c}{2}}\left|\delta_j-\delta_i\right|^{1+c}\end{aligned}\right\} \tag{21}$$

Applying Lemma 2, for $0 < c < 1$, it follows:

$$\left.\begin{aligned}&\left(\sum_{i,j=1}^{N} a_{\lambda ij}^{\frac{1+c}{2}}\left|\delta_j-\delta_i\right|^{1+c}\right)^{\frac{1}{1+c}} \\ &\qquad\geq \left(\sum_{i,j=1}^{N} a_{\lambda ij}\left|\delta_j-\delta_i\right|^2\right)^{\frac{1}{2}}\end{aligned}\right\} \tag{22}$$

Then, applying Lemma 3, it follows:

$$\left.\begin{aligned}\dot{V}_\lambda &\leq -2\Im_2\left(\textstyle\sum_{i,j=1}^{N} a_{\lambda ij}\left|\delta_j-\delta_i\right|^2\right)^{\frac{1+c}{2}} \\ &= -2\Im_2\left[2\delta^T(t)L_\lambda\delta(t)\right]^{\frac{1+c}{2}} \\ &\leq -2\Im_2\left[2\Im_2\delta^T(t)\delta(t)\right]^{\frac{1+c}{2}} \\ &= -2\Im_2\left[V_\lambda(t)\right]^{\frac{1+c}{2}}\end{aligned}\right\} \tag{23}$$

Finally, applying Lemma 4, it follows that the incremental cost consensus is established in a finite-time, T_λ, using the control protocol, given in (17), with $(0 < c < 1)$. Furthermore, in terms of the initial errors, the convergence time, T_λ, can be upper bounded as follows:

$$T_\lambda = \frac{V_\lambda^{\frac{1-c}{2}}(0)}{2\Im_2\left(\frac{1-c}{2}\right)} = \frac{\left[2\Im_2\|\delta(0)\|^2\right]^{\frac{1-c}{2}}}{\Im_2(1-c)} \tag{24}$$

Moreover,

$$\left.\begin{aligned}&\lim_{t\to T_\lambda}\lambda_i(t) = \lambda_j(t) \\ &\text{or } \lambda_i(t) = \lambda_j(t), \quad \text{for all } t \geq T_\lambda\end{aligned}\right\}$$

This completes the proof. □

V. SIMULATION RESULTS AND DISCUSSION

A single-line diagram of the microgrid simulation testbench is shown in Fig. 1 that is operated in the islanded mode to validate the effectiveness of the proposed distributed hierarchical control technique. The information exchange between DGs is represented by a communication graph, $\mathcal{G}$, in the same schematic. Various parameters of the testbench are specified in Appendix, in Tables 2–5. The reference microgrid frequency and voltage are chosen to be 60 Hz and 120.23 V (phase-to-neutral), respectively. Moreover, the standard frequency and voltage tolerances have been chosen, respectively, ±2% and ±5%, as per IEC 60034-1.

For performance assessment, four different tests are conducted:

Test 1: Performance validation of the proposed control strategy for distributed economic load dispatch
Test 2: Performance comparison with the conventional centralized economic load dispatch
Test 3: Scalability assessment of the proposed control strategy
Test 4: Robustness to disturbances

Note that in Tests 1–4, the primary control is enforced through the conventional droop technique, and the secondary control is provided using the distributed strategy. Moreover, in Tests 1, 3 and 4, the tertiary control is provided using the distributed strategy, while in Test 2 it is provided using the centralized strategy. In each case, the system is tested under load variations.

A. HOW DOES THE OVERALL CLOSED-LOOP SYSTEM OPERATE?

The operation of the proposed closed-loop distributed hierarchical control strategy, shown in Fig. 2, is as follows:

- The distributed tertiary controller commands the distributed secondary controller. That is, it generates and dictates the optimal active power dispatch references (i.e., $P_{i,opt}$) to the distributed secondary active power tracking controller.
- Then, the distributed secondary active power tracking controller commands the primary droop controller. That

TABLE 6. Generation cost parameters of DGs illustrated in Fig. 1.

DG Indicator (i)	α_i	β_i	γ_i	P_{min} (kW)	P_{max} (kW)
1	180	6.21	0.0081	0	15
2	200	6.23	0.0083	0	15
3	190	6.22	0.0082	0	12.50

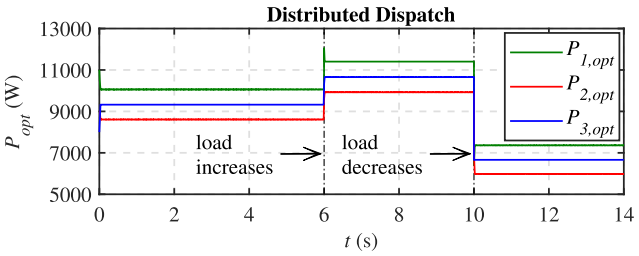

FIGURE 5. Optimal active power dispatch reference signals for DGs.

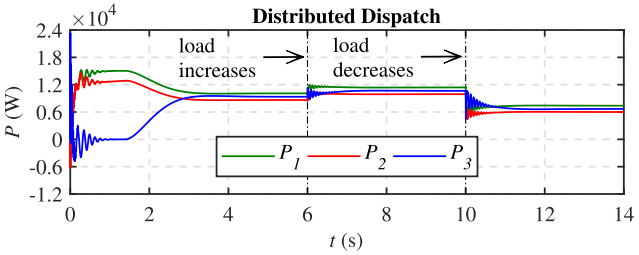

FIGURE 6. Active power outputs of DGs.

is, it generates and dictates new references (i.e., $P_{i,req}$) to the primary controller of each DG.

- In other words, each higher level controller commands and dictates its lower level controller. Consequently, the active power is dispatched economically, the active power demand is completely fulfilled, and the frequencies and output voltages of DGs are regulated to the reference values in a finite-time, despite load variation.

B. TEST 1: PERFORMANCE VALIDATION OF THE PROPOSED CONTROL STRATEGY FOR DISTRIBUTED ECONOMIC LOAD DISPATCH

In Test 1, the total simulation time is kept 14 s. The combined active and reactive power demands are, respectively, as follows: $P_D = 28$ kW and $Q_D = 12$ kVAR during the time interval $t \in [0, 6]$s, that are increased to $P_D = 32$ kW and $Q_D = 16$ kVAR during the time interval $t \in [6, 10]$s, that are again decreased to $P_D = 20$ kW and $Q_D = 8$ kVAR during the time interval $t \in [10, 14]$s. Table 6, indicates various generation cost parameters for each DG. For the distributed secondary controller, the adjustable design parameters, expressed in (4) and (7), are $\kappa_1,\ \kappa_3 = 0.005$ and $\kappa_2,\ \kappa_4 = 0.001$. Similarly, for the distributed tertiary controller, the adjustable design parameters, expressed in (17), are $\kappa_5 = 0.5$, and $c = 0.5$.

Figure 5 indicates the optimal active power dispatch references generated by the distributed tertiary controller, while

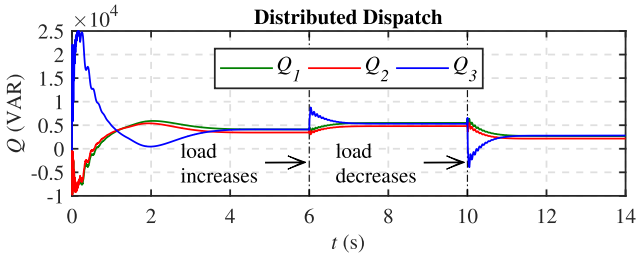

FIGURE 7. Reactive power outputs of DGs.

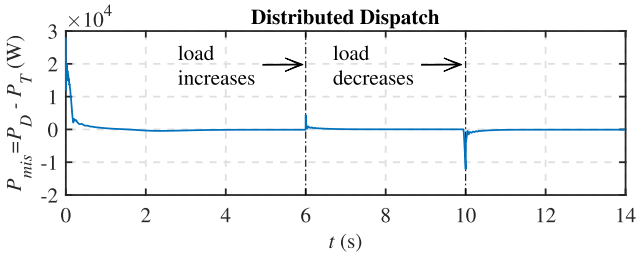

FIGURE 8. Active power mismatch of DGs.

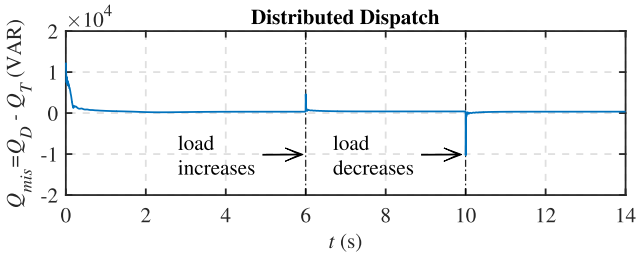

FIGURE 9. Reactive power mismatch of DGs.

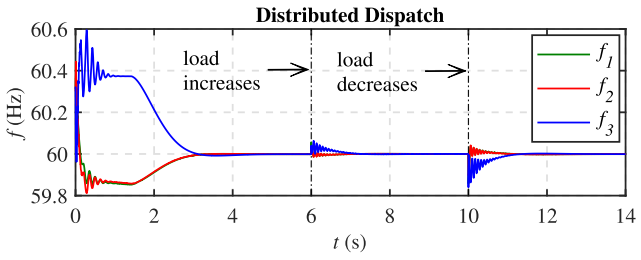

FIGURE 10. Frequencies of DGs.

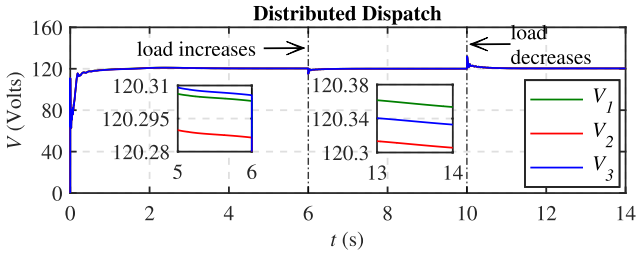

FIGURE 11. Output voltages of DGs.

Figs. 6 and 7, respectively, indicate the corresponding active and reactive power outputs of DGs. Since, both the active

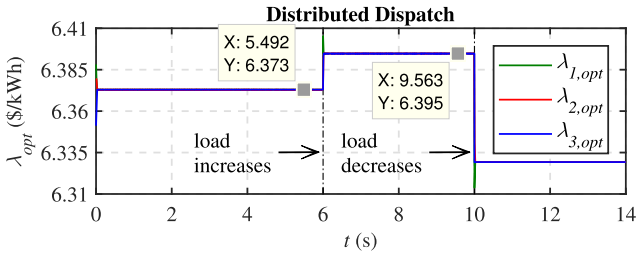

FIGURE 12. Incremental costs of DGs.

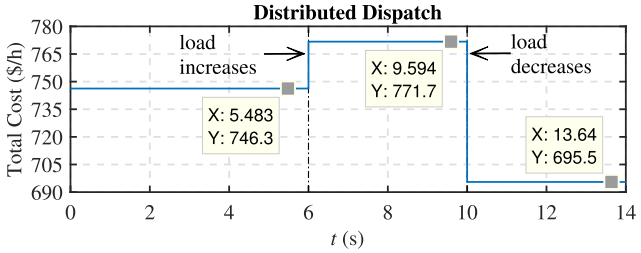

FIGURE 13. Total cost of generation of DGs.

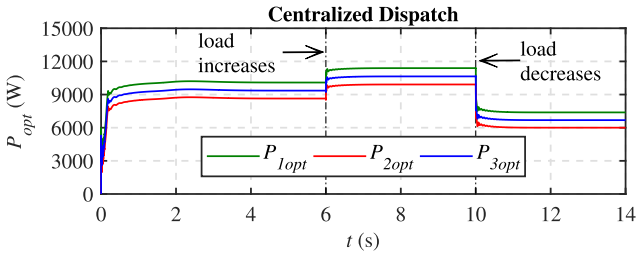

FIGURE 14. Optimal active power dispatch reference signals for DGs.

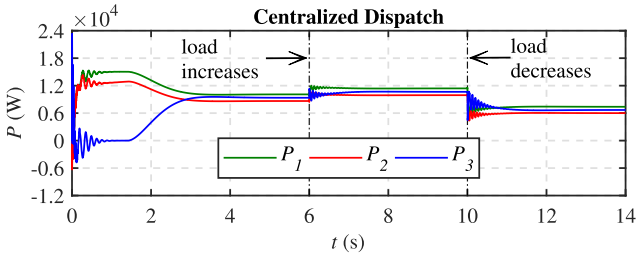

FIGURE 15. Active power outputs of DGs.

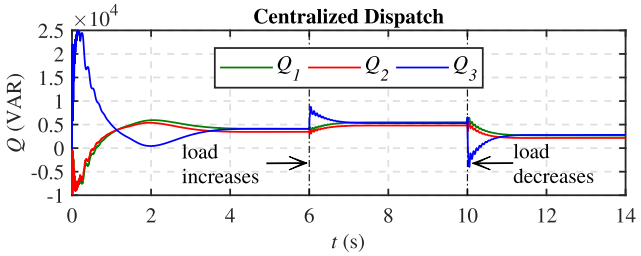

FIGURE 16. Reactive power outputs of DGs.

and reactive power mismatches, as shown in Figs. 8 and 9, respectively, are almost zero (i.e., $P_{mis} = P_D - \sum_{i=1}^{N} P_i = P_D - P_T \approx 0$ and $Q_{mis} = Q_D - \sum_{i=1}^{N} Q_i = Q_D - Q_T \approx 0$), it indicates that the distributed tertiary controller is precisely fulfilling its task. In addition, since the frequencies and output voltages of DGs are converging to the reference values (i.e., 60 Hz and 120.23 V phase-to-neutral, respectively), as shown in Figs. 10 and 11, respectively, it indicates that the distributed secondary controller is also precisely fulfilling its frequency and voltage regulation tasks, despite load variation. Figures 12 and 13, respectively, indicate the incremental costs, λ_{opt}, and the corresponding total generation cost, $\sum_{i=1}^{N} C_i$, of DGs. It is evident that both the incremental costs and the total generation cost of DGs increase under the load increase event due to increased active power dispatch, and vice versa.

C. TEST 2: PERFORMANCE COMPARISON WITH THE CONVENTIONAL CENTRALIZED ECONOMIC LOAD DISPATCH

In Test 2, the total simulation time, the active and reactive power demands and their variations are kept the same as described in Test 1. Having these conditions, the performance of the proposed tertiary controller (i.e., the distributed economic load dispatch scheme) is compared with the centralized tertiary controller (i.e., the centralized economic dispatch strategy), described in Section IV.C1., and reported in reputed power system analysis and control related textbooks [46], [47].

Figure 14 represents the optimal active power dispatch reference signals generated by the centralized tertiary controller, whereas Figs. 15 and 16, respectively, illustrate the corresponding active and reactive power outputs of DGs. It is evident that the optimal active power dispatch references generated by the centralized tertiary controller have a slower convergence than the references generated by the proposed distributed tertiary controller, as shown in Fig. 5. The active and reactive power mismatches in case of the centralized tertiary controller are, respectively, shown in Figs. 17 and 18, which are almost the same as they are in case of the distributed tertiary controller, and shown in Figs. 8 and 9. Similarly, the frequencies of DGs, output voltages of DGs, the incremental costs of DGs, and the total generation cost in case of the centralized tertiary control are, respectively, shown in Figs. 19, 20, 21 and 22, which are nearly the same as they are under the distributed tertiary controller, and shown in Figs. 10, 11, 12 and 13.

After a detailed comparison, one can easily conclude that the proposed distributed tertiary controller provides a comparable performance with the centralized tertiary controller, although having a much lower cost of the communication network. It means that the proposed distributed tertiary controller provides a better solution than the centralized version of the same controller.

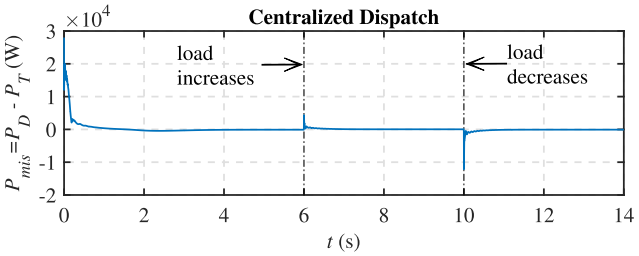

FIGURE 17. Active power mismatch of DGs.

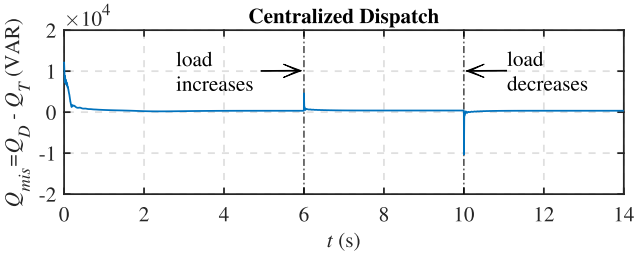

FIGURE 18. Reactive power mismatch of DGs.

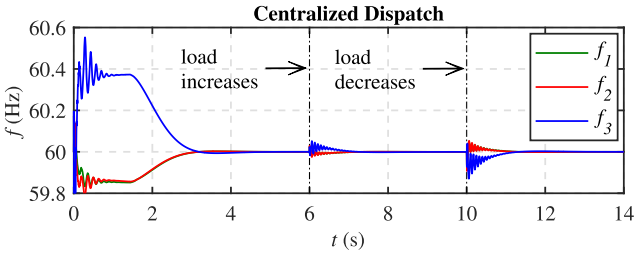

FIGURE 19. Frequencies of DGs.

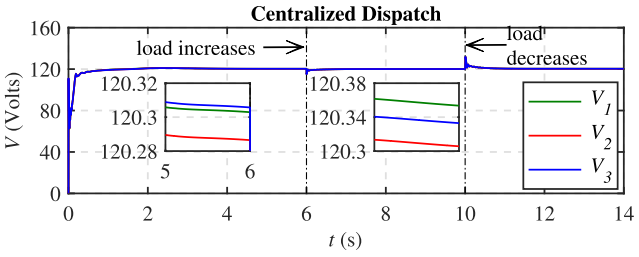

FIGURE 20. Output voltages of DGs.

D. TEST 3: SCALABILITY ASSESSMENT OF THE PROPOSED CONTROL STRATEGY

The scalability of the proposed hierarchical control scheme is verified by applying it to a large islanded AC microgrid comprising 12 inverter-interfaced DGs, as depicted in Fig. 23. The overall active and reactive power demands are, respectively, as follows: $P_D = 80$ kW and $Q_D = 80$ kVAR during the time interval $t \in [0, 7]$s, that are increased to $P_D = 96$ kW and $Q_D = 96$ kVAR during the time interval $t \in [7, 11]$s, that are again decreased to $P_D = 72$ kW and $Q_D = 72$ kVAR during the time interval $t \in [11, 15]$s. Table 7, indicates various generation cost parameters for each DG shown in Fig. 23. Figure 24 depicts the optimal active power dispatch references generated by the distributed tertiary controller, while Fig. 25 indicates the corresponding active power outputs of DGs. Since, both the active and reactive power mismatches, as shown in Figs. 26 and 27, respectively, are converging to near zero, it means that both the active and reactive power demands are reasonably fulfilled with tolerable mismatches. In addition, since the frequencies and output voltages of DGs are converging to the reference values, as depicted in Figs. 28 and 29, respectively, it indicates that the distributed secondary controller is also precisely fulfilling its frequency and voltage regulation tasks, despite load variation. Figures 30 and 31, respectively, indicate the incremental costs, λ_{opt}, and the corresponding total generation cost of DGs. It is evident that both the incremental costs and the total generation cost of DGs increase under the load increase event due to increased active power dispatch, and vice versa.

TABLE 7. Generation cost parameters of DGs illustrated in Fig. 23.

DG Indicator (i)	α_i	β_i	γ_i	P_{min} (kW)	P_{max} (kW)
1	180	6.21	0.0081	0	15
2	200	6.23	0.0083	0	15
3	190	6.22	0.0082	0	15
4	210	6.24	0.0084	0	15
5	230	6.26	0.0086	0	15
6	220	6.25	0.0085	0	15
7	240	6.27	0.0087	0	15
8	260	6.29	0.0089	0	15
9	250	6.28	0.0088	0	15
10	270	6.30	0.0090	0	15
11	290	6.32	0.0092	0	15
12	280	6.31	0.0091	0	15

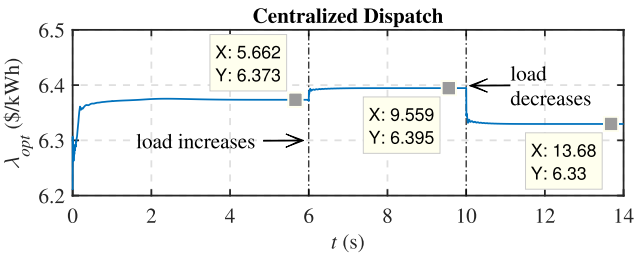

FIGURE 21. Incremental costs of DGs.

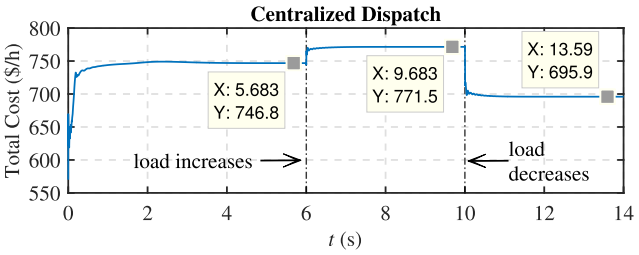

FIGURE 22. Total cost of generation of DGs.

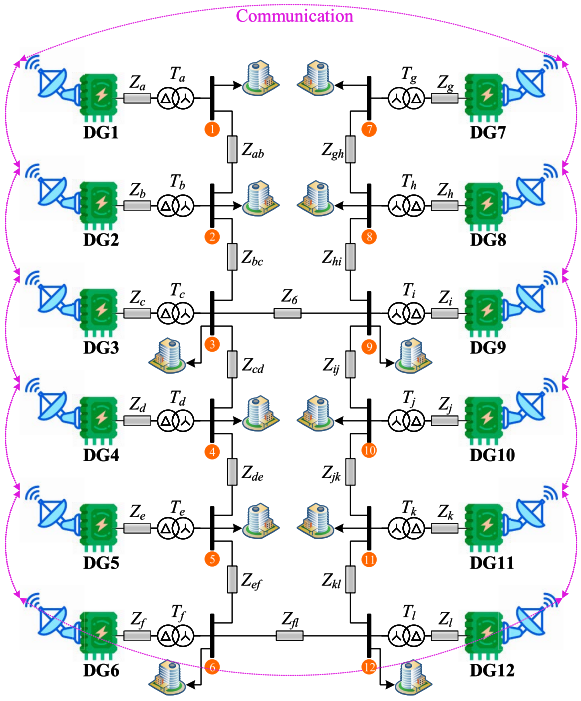

FIGURE 23. Large microgrid testbench for scalability assessment.

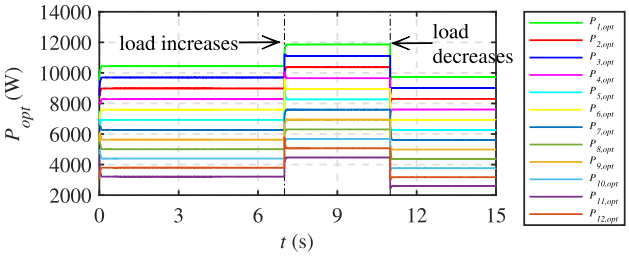

FIGURE 24. Optimal active power dispatch reference signals for DGs.

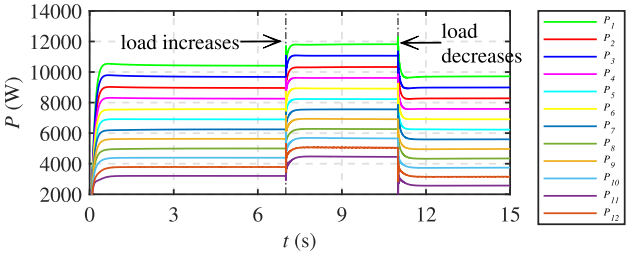

FIGURE 25. Active power outputs of DGs.

E. TEST 4: ROBUSTNESS TO DISTURBANCES

To verify the robustness of the proposed scheme to disturbances, a sinusoidal disturbance is injected into the quantity $P_{1,opt}$ during the time interval $t \in [6, 8]$s, such that $P^{New}_{1,opt} = P_{1,opt} + \sin 10t \ \forall \ (6 \leq t \leq 8)$s. This disturbance can easily be seen with a naked eye in the optimal active power dispatch reference signals, the active power outputs of DGs, the reactive power outputs of DGs and the frequencies of DGs, respectively, shown in Figs. 32, 33, 34, and 35. Although it

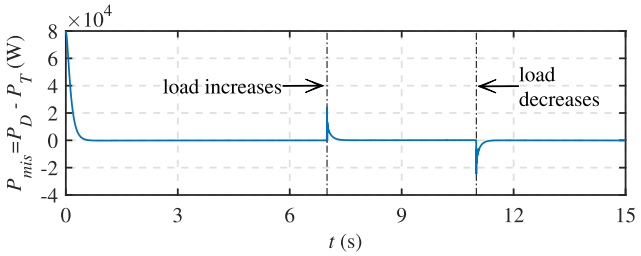

FIGURE 26. Active power mismatch of DGs.

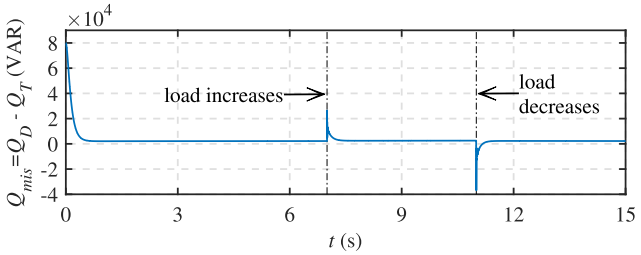

FIGURE 27. Reactive power mismatch of DGs.

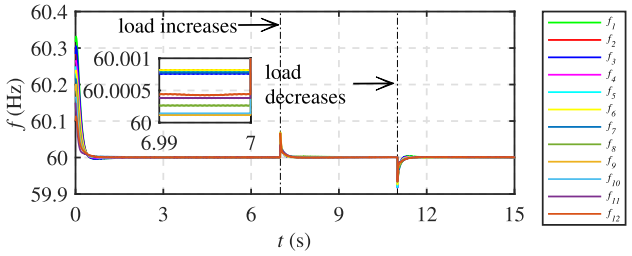

FIGURE 28. Frequencies of DGs.

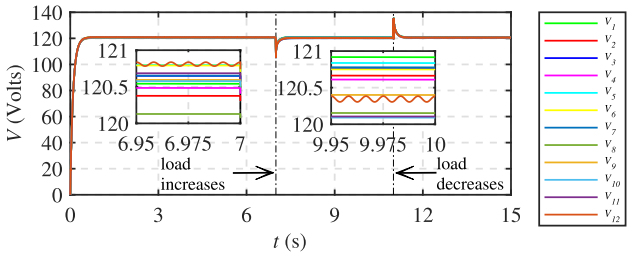

FIGURE 29. Output voltages of DGs.

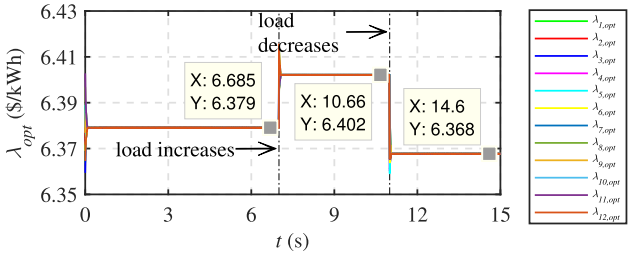

FIGURE 30. Incremental costs of DGs.

is not recognizable with a naked eye in the output voltages and the incremental costs of DGs, respectively, shown in Figs. 36 and 37. It is evident that once the disturbance is removed, the proposed strategy quickly restores both the

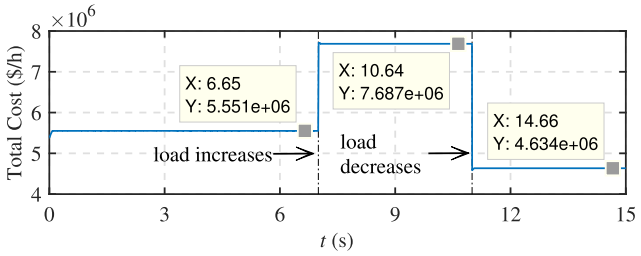

FIGURE 31. Total cost of generation of DGs.

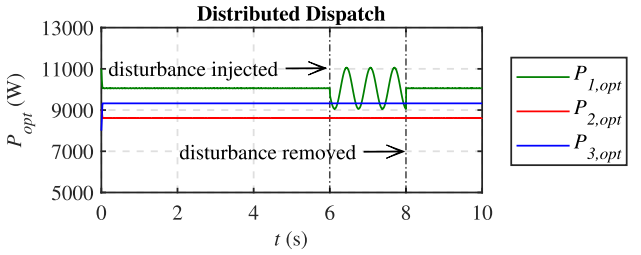

FIGURE 32. Optimal active power dispatch reference signals for DGs.

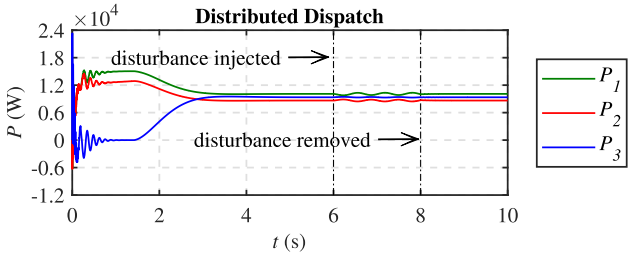

FIGURE 33. Active power outputs of DGs.

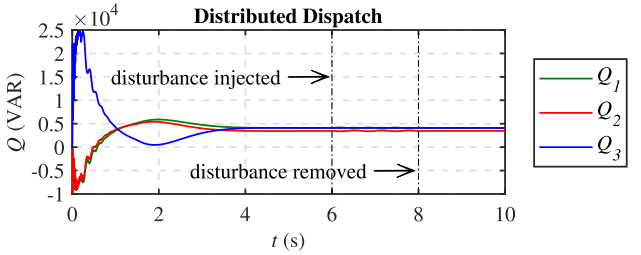

FIGURE 34. Reactive power outputs of DGs.

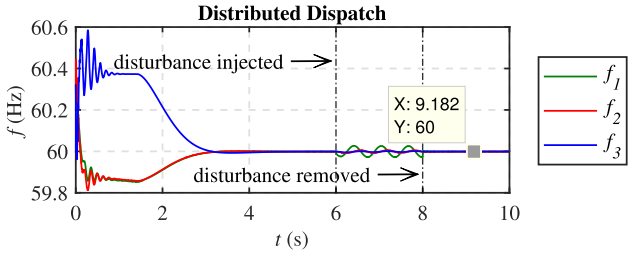

FIGURE 35. Frequencies of DGs.

frequencies and voltages of DGs to their reference values in a finite-time, and concurrently ensures the economic load dispatch. This is a clear indication of the robustness of the proposed scheme to disturbances.

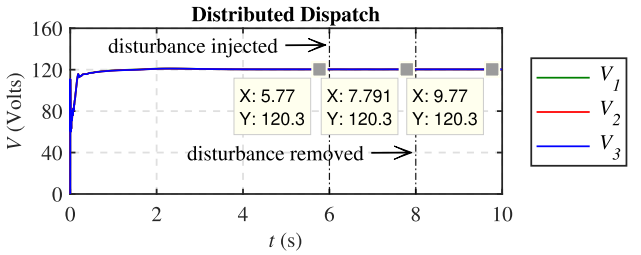

FIGURE 36. Output voltages of DGs.

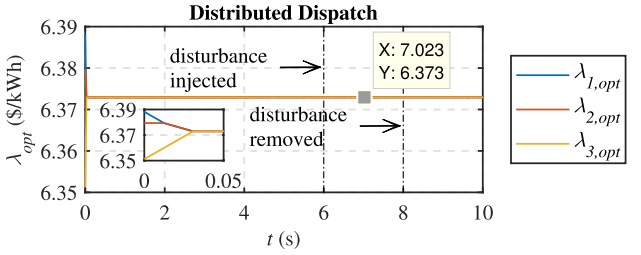

FIGURE 37. Incremental costs of DGs.

VI. CONCLUSION

This article presents a fully distributed three-layered hierarchical control scheme applicable to islanded AC microgrids. Due to the fully distributed design, the computation and communication burden is shared between the neighboring DGs using a sparse communication network. Consequently, the proposed paradigm is not susceptible to the single-point-failure issue, like the contemporary conventional centralized or distributed leader-follower based hierarchical control techniques. The proposed strategy fulfills multiples control objectives simultaneously, including: (i) frequency and voltage regulation of DGs within the prescribed frequency and voltage deviation limits as per IEC 60034-1 standard (i.e., $\pm 2\%$ and $\pm 5\%$, respectively) without requiring any leader-follower consensus at the secondary level, (ii) distributed economic dispatch of active power with a negligible error, and (iii) reactive power dispatch with a plausible error. The stated control objectives have been successfully achieved by evaluating the performance of the proposed scheme in Matlab/Simulink through various time-domain based numerical simulations under different loading conditions and microgrid expansion. Based on its excellent dynamic performance and accomplishment of the control objectives, the proposed strategy testifies itself to be an effective hierarchical control strategy for islanded AC microgrids.

REFERENCES

[1] D. T. Ton and M. A. Smith, "The U.S. department of energy's microgrid initiative," *Electr. J.*, vol. 25, no. 8, pp. 84–94, 2012.
[2] N. Hatziargyriou, *Microgrids: Architectures and Control*. Hoboken, NJ, USA: Wiley, 2014.
[3] D. E. Olivares, A. Mehrizi-Sani, A. H. Etemadi, C. A. Cañizares, R. Iravani, M. Kazerani, A. H. Hajimiragha, O. Gomis-Bellmunt, M. Saeedifard, R. Palma-Behnke, G. A. Jiménez-Estévez, and N. D. Hatziargyriou, "Trends in microgrid control," *IEEE Trans. Smart Grid*, vol. 5, no. 4, pp. 1905–1919, Jul. 2014.

[4] A. Bidram and A. Davoudi, "Hierarchical structure of microgrids control system," *IEEE Trans. Smart Grid*, vol. 3, no. 4, pp. 1963–1976, Dec. 2012.
[5] *IEEE Standard for the Specification of Microgrid Controllers*, IEEE Standard 2030.7-2017, Apr. 2018, pp. 1–43, doi: 10.1109/IEEESTD.2018.8340204.
[6] J. M. Guerrero, J. C. Vasquez, J. Matas, L. G. de Vicuna, and M. Castilla, "Hierarchical control of droop-controlled AC and DC microgrids—A general approach toward standardization," *IEEE Trans. Ind. Electron.*, vol. 58, no. 1, pp. 158–172, Jan. 2011.
[7] J. C. Vasquez, J. M. Guerrero, J. Miret, M. Castilla, and L. G. De Vicuna, "Hierarchical control of intelligent microgrids," *IEEE Ind. Electron. Mag.*, vol. 4, no. 4, pp. 23–29, Dec. 2010.
[8] E. Planas, A. Gil-de-Muro, J. Andreu, I. Kortabarria, and I. M. de Alegría, "General aspects, hierarchical controls and droop methods in microgrids: A review," *Renew. Sustain. Energy Rev.*, vol. 17, pp. 147–159, Jan. 2013.
[9] M. Farrokhabadi *et al.*, "Microgrid stability definitions, analysis, and examples," *IEEE Trans. Power Syst.*, vol. 35, no. 1, pp. 13–29, Jan. 2020.
[10] A. Vasilakis, I. Zafeiratou, D. T. Lagos, and N. D. Hatziargyriou, "The evolution of research in microgrids control," *IEEE Open Access J. Power Energy*, vol. 7, pp. 331–343, 2020.
[11] N. M. Dehkordi, N. Sadati, and M. Hamzeh, "Distributed robust finite-time secondary voltage and frequency control of islanded microgrids," *IEEE Trans. Power Syst.*, vol. 32, no. 5, pp. 3648–3659, Sep. 2017.
[12] Y. Khayat, Q. Shafiee, R. Heydari, M. Naderi, T. Dragicevic, J. W. Simpson-Porco, F. Dorfler, M. Fathi, F. Blaabjerg, J. M. Guerrero, and H. Bevrani, "On the secondary control architectures of AC microgrids: An overview," *IEEE Trans. Power Electron.*, vol. 35, no. 6, pp. 6482–6500, Jun. 2020.
[13] O. Palizban and K. Kauhaniemi, "Hierarchical control structure in microgrids with distributed generation: Island and grid-connected mode," *Renew. Sustain. Energy Rev.*, vol. 44, pp. 797–813, Apr. 2015.
[14] A. Bidram, A. Davoudi, F. L. Lewis, and J. M. Guerrero, "Distributed cooperative secondary control of microgrids using feedback linearization," *IEEE Trans. Power Syst.*, vol. 28, no. 3, pp. 3462–3470, Aug. 2013.
[15] A. Bidram, F. L. Lewis, and A. Davoudi, "Distributed control systems for small-scale power networks: Using multiagent cooperative control theory," *IEEE Control Syst. Mag.*, vol. 34, no. 6, pp. 56–77, Dec. 2014.
[16] A. Pilloni, A. Pisano, and E. Usai, "Robust finite-time frequency and voltage restoration of inverter-based microgrids via sliding-mode cooperative control," *IEEE Trans. Ind. Electron.*, vol. 65, no. 1, pp. 907–917, Jan. 2018.
[17] S. D'Silva, M. B. Shadmand, and H. Abu-Rub, "Microgrid control strategies for seamless transition between grid-connected and islanded modes," in *Proc. IEEE Texas Power Energy Conf. (TPEC)*, College Station, TX, USA, Feb. 2020, pp. 1–6.
[18] J. M. Guerrero, M. Chandorkar, T.-L. Lee, and P. C. Loh, "Advanced control architectures for intelligent microgrids—Part I: Decentralized and hierarchical control," *IEEE Trans. Ind. Electron.*, vol. 60, no. 4, pp. 1254–1262, Apr. 2013.
[19] N. M. Dehkordi, H. R. Baghaee, N. Sadati, and J. M. Guerrero, "Distributed noise-resilient secondary voltage and frequency control for islanded microgrids," *IEEE Trans. Smart Grid*, vol. 10, no. 4, pp. 3780–3790, Jul. 2019.
[20] Z. Li, C. Zang, P. Zeng, H. Yu, and S. Li, "Fully distributed hierarchical control of parallel grid-supporting inverters in islanded AC microgrids," *IEEE Trans. Ind. Electron.*, vol. 14, no. 2, pp. 679–690, Feb. 2018.
[21] Z. Zhao, P. Yang, J. M. Guerrero, Z. Xu, and T. C. Green, "Multiple-time-scales hierarchical frequency stability control strategy of medium-voltage isolated microgrid," *IEEE Trans. Power Electron.*, vol. 31, no. 8, pp. 5974–5991, Aug. 2016.
[22] A. La Bella, S. R. Cominesi, C. Sandroni, and R. Scattolini, "Hierarchical predictive control of microgrids in islanded operation," *IEEE Trans. Autom. Sci. Eng.*, vol. 14, no. 2, pp. 536–546, Apr. 2017.
[23] X. Wu, L. Chen, C. Shen, Y. Xu, J. He, and C. Fang, "Distributed optimal operation of hierarchically controlled microgrids," *IET Gener., Transmiss. Distrib.*, vol. 12, no. 18, pp. 4142–4152, Oct. 2018.
[24] X. Hou, Y. Sun, J. Lu, X. Zhang, L. H. Koh, M. Su, and J. M. Guerrero, "Distributed hierarchical control of AC microgrid operating in grid-connected, islanded and their transition modes," *IEEE Access*, vol. 6, pp. 77388–77401, 2018.
[25] Q. Zhou, M. Shahidehpour, Z. Li, and X. Xu, "Two-layer control scheme for maintaining the frequency and the optimal economic operation of hybrid AC/DC microgrids," *IEEE Trans. Power Syst.*, vol. 34, no. 1, pp. 64–75, Jan. 2019.
[26] F. Mehmood, B. Khan, S. M. Ali, and J. A. Rossiter, "Distributed model predictive based secondary control for economic production and frequency regulation of MG," *IET Control Theory Appl.*, vol. 13, no. 17, pp. 2948–2958, Nov. 2019.
[27] J. M. Rey, P. P. Vergara, M. Castilla, A. Camacho, M. Velasco, and P. Martí, "Droop-free hierarchical control strategy for inverter-based AC microgrids," *IET Power Electron.*, vol. 13, no. 7, pp. 1403–1415, May 2020.
[28] Z. Cheng, Z. Li, J. Liang, J. Si, L. Dong, and J. Gao, "Distributed coordination control strategy for multiple residential solar PV systems in distribution networks," *Int. J. Electr. Power Energy Syst.*, vol. 117, May 2020, Art. no. 105660.
[29] Z. Li, Z. Cheng, J. Liang, J. Si, L. Dong, and S. Li, "Distributed event-triggered secondary control for economic dispatch and frequency restoration control of droop-controlled AC microgrids," *IEEE Trans. Sustain. Energy*, vol. 11, no. 3, pp. 1938–1950, Jul. 2020.
[30] F. Mehmood, B. Khan, S. M. Ali, M. B. Qureshi, C. Diver, and R. Nawaz, "Multi-renewable energy agent based control for economic dispatch and frequency regulation of autonomous renewable grid," *IEEE Access*, vol. 8, pp. 89534–89545, 2020.
[31] F. Mehmood, B. Khan, and S. M. Ali, "Renewable generation intermittence and economic dispatch control of autonomous microgrid with distributed sliding mode," *Int. J. Electr. Power Energy Syst.*, vol. 130, Sep. 2021, Art. no. 106937.
[32] F. Mehmood, B. Khan, S. M. Ali, and J. A. Rossiter, "Distributed MPC for economic dispatch and intermittence control of renewable based autonomous microgrid," *Electr. Power Syst. Res.*, vol. 195, Jun. 2021, Art. no. 107131.
[33] T.-L. Nguyen, Y. Wang, Q.-T. Tran, R. Caire, Y. Xu, and C. Gavriluta, "A distributed hierarchical control framework in islanded microgrids and its agent-based design for cyber–physical implementations," *IEEE Trans. Ind. Electron.*, vol. 68, no. 10, pp. 9685–9695, Oct. 2021.
[34] Z. Li, Z. Cheng, J. Si, and S. Li, "Distributed event-triggered hierarchical control to improve economic operation of hybrid AC/DC microgrids," *IEEE Trans. Power Syst.*, early access, Dec. 27, 2021, doi: 10.1109/TPWRS.2021.3133487.
[35] Z. Zhang, Y. Mishra, D. Yue, C. Dou, B. Zhang, and Y.-C. Tian, "Delay-tolerant predictive power compensation control for photovoltaic voltage regulation," *IEEE Trans. Ind. Informat.*, vol. 17, no. 7, pp. 4545–4554, Jul. 2021.
[36] Z. Zhang, C. Dou, D. Yue, and B. Zhang, "Predictive voltage hierarchical controller design for islanded microgrids under limited communication," *IEEE Trans. Circuits Syst. I, Reg. Papers*, vol. 69, no. 2, pp. 933–945, Feb. 2022.
[37] S. Ullah, L. Khan, I. Sami, G. Hafeez, and F. R. Albogamy, "A distributed hierarchical control framework for economic dispatch and frequency regulation of autonomous AC microgrids," *Energies*, vol. 14, no. 24, p. 8408, Dec. 2021.
[38] A. Bidram, V. Nasirian, A. Davoudi, and F. L. Lewis, *Cooperative Synchronization in Distributed Microgrid Control*. Cham, Switzerland: Springer, 2017.
[39] J. A. Bondy and U. S. R. Murty, *Graph Theory*. London, U.K.: Springer-Verlag, 2008.
[40] M. J. Erickson and R. H. Lasseter, "Integration of battery energy storage element in a CERTS microgrid," in *Proc. IEEE Energy Convers. Congr. Expo.*, Atlanta, GA, USA, Sep. 2010, pp. 2570–2577.
[41] R. H. Lasseter and P. Piagi, "Control and design of microgrid components," Power Syst. Eng. Res. Center (PSERC), Univ. Wisconsin-Madison, Madison, WI, USA, Tech. Rep. 06–03, 2006. Accessed: Jun. 22, 2021. [Online]. Available: https://certs.lbl.gov/sites/all/files/ctrl-design-microgrid-components.pdf
[42] W. Du and R. H. Lasseter, "Overload mitigation control of droop-controlled grid-forming sources in a microgrid," in *Proc. IEEE Power Energy Soc. Gen. Meeting*, Chicago, IL, USA, Jul. 2017, pp. 1–5.
[43] F. Chen, Y. Cao, and W. Ren, "Distributed average tracking of multiple time-varying reference signals with bounded derivatives," *IEEE Trans. Autom. Control*, vol. 57, no. 12, pp. 3169–3174, Dec. 2012.
[44] A. Polyakov and A. Poznyak, "Lyapunov function design for finite-time convergence analysis: 'Twisting' controller for second-order sliding mode realization," *Automatica*, vol. 45, no. 2, pp. 444–448, Feb. 2009.
[45] J. Cortés, "Discontinuous dynamical systems," *IEEE Control Syst. Mag.*, vol. 28, no. 3, pp. 36–73, May 2008.
[46] H. Saadat, *Power System Analysis*. Alexandria, VA, USA: PSA Publishing, 2010.

[47] A. J. Wood, B. F. Wollenberg, and G. B. Sheblé, *Power Generation, Operation, and Control*, Hoboken, NJ, USA: Wiley, 2013.
[48] X. Liu, J. Lam, W. Yu, and G. Chen, "Finite-time consensus of multiagent systems with a switching protocol," *IEEE Trans. Neural Netw. Learn. Syst.*, vol. 27, no. 4, pp. 853–862, Apr. 2016.
[49] G. H. Hardy, J. E. Littlewood, G. Pólya, and G. Pólya, *Inequalities*. Cambridge, U.K.: Cambridge Univ. Press, 1952.
[50] H. Zhang, F. L. Lewis, and Z. Qu, "Lyapunov, adaptive, and optimal design techniques for cooperative systems on directed communication graphs," *IEEE Trans. Ind. Electron.*, vol. 59, no. 7, pp. 3026–3041, Jul. 2012.
[51] M. Forti, M. Grazzini, P. Nistri, and L. Pancioni, "Generalized Lyapunov approach for convergence of neural networks with discontinuous or non-Lipschitz activations," *Phys. D, Nonlinear Phenomena*, vol. 214, no. 1, pp. 88–99, Feb. 2006.

SHAFAAT ULLAH was born in Lakki Marwat, Pakistan. He received the B.Sc. and M.Sc. degrees in electrical engineering from the University of Engineering and Technology Peshawar, Pakistan, in 2007 and 2013, respectively. He is currently pursuing the Ph.D. degree in electrical engineering with COMSATS University Islamabad, Abbottabad Campus, Abbottabad, Pakistan.

He has worked as an Assistant Director for the Pakistan Council of Renewable Energy Technologies (PCRET), and as an Assistant Manager (Operation)/a Junior Engineer (Electrical) for Lahore Electric Supply Company (LESCO), Pakistan. He is currently working as an Assistant Professor with the Department of Electrical Engineering, University of Engineering and Technology Peshawar, Bannu Campus, Pakistan. His research interests include photovoltaics, wind energy conversion systems, and distributed control of multi-agent systems-based smart grids.

LAIQ KHAN received the B.Sc. degree (Hons.) in electrical engineering from the University of Engineering and Technology Peshawar, Peshawar, Pakistan, in 1996, and the M.S.-leading-to-Ph.D. degree in power system dynamics and control from the University of Strathclyde, Glasgow, U.K., in 2003.

Before Ph.D. degree, he served for Siemens Pakistan as a Field Engineer, for two years. He worked as an Assistant Professor with the Faculty of Electronic Engineering, Ghulam Ishaq Khan Institute of Engineering Sciences and Technology, Swabi, Pakistan, until 2008. Then, he joined the Faculty of Electrical Engineering, COMSATS University Islamabad, Abbottabad Campus, Pakistan, and worked as an Associate Professor. He also worked as a Professor with Islamic University Madinah, Saudi Arabia, for three years. He is currently a Professor in power system dynamics and control with COMSATS University Islamabad. He has published more than 100 papers in highly reputable international conferences and peer-reviewed impact factor journals. His research interests include power system stability and control using PSSs, FACTS controllers and HVDC, robust control theory, intelligent control systems, nonlinear adaptive intelligent control and adaptive predictive intelligent control, fault tolerant control, power system planning and advanced optimization techniques, nonlinear control of wecs, photovoltaic systems, micro-grids, and smart-grids.

IRFAN SAMI received the B.Sc. degree in electrical engineering from the University of Engineering and Technology Peshawar, Bannu Campus, Pakistan, in 2016, and the M.Sc. degree in electrical engineering from COMSATS University Islamabad, Abbottabad Campus, Abbottabad, Pakistan, in 2019. He is currently pursuing the Ph.D. degree in electrical engineering with Chung-Ang University, Seoul, South Korea. His research interests include electric drives, renewable energies, and electrical machines design.

JONG-SUK RO received the B.S. degree in mechanical engineering from Hanyang University, Seoul, South Korea, in 2001, and the Ph.D. degree in electrical engineering from Seoul National University (SNU), Seoul, in 2008.

From 2008 to 2012, he conducted research with the Research and Development Center, Samsung Electronics, as a Senior Engineer. From 2012 to 2013, he was with the Brain Korea 21 Information Technology, SNU, as a Postdoctoral Fellow. He conducted research with the Electrical Energy Conversion System Research Division, Korea Electrical Engineering and Science Research Institute, as a Researcher, in 2013. From 2013 to 2016, he worked with the Brain Korea 21 Plus, SNU, as a BK Assistant Professor. In 2014, he was with the University of Bath, Bath, U.K. He is currently an Associate Professor with the School of Electrical and Electronics Engineering, Chung-Ang University, Seoul. His research interests include the analysis and optimal design of next-generation electrical machines using smart materials, such as electromagnet, piezoelectric, and magnetic shape memory alloy.